

Article

Thermoelastic Analysis of Functionally Graded Cylindrical Panels with Piezoelectric Layers

Yasin Heydarpour ¹, Parviz Malekzadeh ^{1,*} , Rossana Dimitri ²  and Francesco Tornabene ^{2,*} 

¹ Department of Mechanical Engineering, School of Engineering, Persian Gulf University, Bushehr 7516913817, Iran; Heydarpour@aut.ac.ir

² Department of Innovation Engineering, University of Salento, Via per Monteroni, 73100 Lecce, Italy; rossana.dimitri@unisalento.it

* Correspondence: malekzadeh@pgu.ac.ir (P.M.); francesco.tornabene@unisalento.it (F.T.)

Received: 18 January 2020; Accepted: 13 February 2020; Published: 19 February 2020



Abstract: We propose a coupled thermoelastic approach based on the Lord-Shulman (L-S) and Maxwell's formulations to study the wave propagation in functionally graded (FG) cylindrical panels with piezoelectric layers under a thermal shock loading. The material properties of the FG core layer feature a graded distribution throughout the thickness and vary according to a simple power law. A layerwise differential quadrature method (LW-DQM) is combined with a non-uniform rational B-spline (NURBS) multi-step time integration scheme to discretize the governing equations both in the spatial and time domains. The compatibility conditions of the physical quantities are enforced at the interfaces to describe their structural behavior in a closed form. A validation and comparative analysis with the available literature, together with a convergence study, show the efficiency and stability of the proposed method to handle thermoelastic problems. Numerical applications are herein performed systematically to check for the sensitivity of the thermoelastic response to the material graded index, piezoelectric layer thickness, external electrical voltage, opening angle, and shock thermal loading, which would be very helpful for practical engineering applications.

Keywords: Lord-Shulman thermoelasticity; cylindrical panels; functionally graded; Piezoelectric layers; LW-DQM; Multi-step time integration scheme

1. Introduction

Functionally graded (FG) cylindrical panels are largely used as structural members in many industrial applications such as aerospace vehicles, nuclear equipment, petro-chemical structures, among others. FG structures usually operate under high thermal conditions, which can yield a vibratory motion, especially when subjected to a sudden variation of the thermal conditions. On the other hand, the mechanical behavior and the vibration control of FG cylindrical panels can be improved by introducing piezoelectric layers at their inner and/or outer surfaces. This requires an accurate evaluation of the thermoelastic properties of FG cylindrical panels, with attached piezoelectric layers under a thermal shock loading, for design and manufacturing purposes.

In this context, it is well known that a conventional Fourier heat conduction law is unable to predict the temperature distribution and heat wave propagation within a continuum at the initial phase. On the other hand, an uncoupled classical thermoelastic approach cannot accurately predict the thermoelastic behavior of a body under a thermal shock. Countermeasures against these limitations have encouraged the development of different coupled thermoelasticity theories [1–3]. Among them, the Lord and Shulman (L-S) generalized thermoelasticity theory is one of the simplest formulations applied in the literature [4–14], which includes a relaxation time and a coupling between thermal and mechanical energies [1]. In this framework, some interesting thermoelastic studies based on an

uncoupled classical thermoelasticity theory of FG cylindrical panels and shells can be found in [15–31]. These studies considered the possible presence of piezoelectric layers, and estimated the temperature distribution of a body by means of a Fourier heat conduction law. On the other hand, many works, in literature, have applied a non-Fourier heat transfer law or coupled theories to study the thermoelastic response of FG structures [32–37]. More specifically, Entezari et al. [32] explored the capabilities of a refined finite element approach based on the L-S generalized theory of thermoelasticity and Carrera Unified Formulation (CUF) for the 3D thermoelastic analysis of FG disks exposed to a thermal shock loading. Zhang et al. [33] employed a generalized fractional Cattaneo-type heat conduction model to analyze the thermal shock problem of elastic FG strips with internal cracks, while using a Fourier and Laplace transforms for an analytical computation of the thermoelastic field unknowns. Sator et al. [34] presented a unified formulation for the bending response of FG plates under a transient thermal loading in the framework of the L-S generalized thermoelasticity and two-dimensional plate theories. In their work, the authors applied a meshless method and a Wilson time integration scheme to solve numerically the governing equations of the problem. In line with the previous works, Pourasghar and Chen [35] applied the non-Fourier heat conduction equations to determine the temperature distribution and the induced thermal stresses and deformations, in carbon nanotube-reinforced composite cylindrical panels subjected to a heat pulse. They assumed temperature-dependent material properties and applied a differential quadrature method (DQM) to discretize the governing equations and solve the problem numerically. Heydarpour and Malekzadeh [36] studied the propagation of thermoelastic waves in laminated spherical shells with temperature-dependent material properties and FG layers under thermal boundary conditions according to the L-S generalized thermoelasticity. Heydarpour et al. [37] investigated the thermo-mechanical wave propagation in composite spherical shells reinforced with multilayer functionally graded graphene platelets under a thermo-mechanical shock loading. They formulated the problem in the context of L-S thermoelasticity together with a layerwise (LW) DQM, where the governing equations were solved in the time domain both analytically and numerically. The non-linear behavior of the shell structures under different loading conditions, makes the wave propagation problem particularly sensitive to the selected mechanical and geometrical parameters. This represents a key aspect of higher-order numerical approaches for shell structures [38–43].

To date, however, there has been a general lack of works applying coupled thermoelastic approaches to FG cylindrical panels with surface piezoelectric layers under a thermal shock. Due to its practical importance and usefulness from a research and practical engineering standpoint, this issue is investigated in the present paper. In order to describe the high transient nature of a thermal loading, especially at the initial phase of its application, the problem is formulated according to the L-S thermoelasticity theory, with a special emphasis on the heat wave propagation. The material properties of FG panels are assumed to vary throughout the thickness, and a layerwise (LW) approach is adopted to simulate the variation of field variables throughout the thickness, due to its high accuracy and computational efficiency compared to a conventional finite element method (FEM) or finite difference method (FDM), as verified for different engineering problems. The LW theory, indeed, has been largely proved to be an efficient tool for the study of the response and transverse the shear and normal stress distributions of laminated composites. It represents a refined approach that considers the effects of thickness at a reduced computational cost. Based on a LW theory, the shear strains are discontinuous, and hence the shear stresses can be continuous at the interface of two adjacent layers. This represents a clear advantage of the LW approach with respect to higher order shear deformation theories. At the same time, the successful employment of the DQM for different structural and fluid problems has largely been proved in literature [11,20,36,43–52].

Accordingly, a LW-DQM is proposed to discretize the governing equations in the spatial domain, which are solved using a multi-step Non-Uniform-Rational-B-Spline (NURBS)-based technique. The correctness and accuracy of the present approach is endowed with a convergence study and comparative analysis of results with respect to the available predictions from the literature in the limit cases. Afterward, the effect of the material gradient index, relaxation time, opening angle,

piezoelectric layer thickness, and external electrical voltage on the thermoelastic behavior of the system is investigated parametrically.

The outline of the paper is as follows: in Section 2 we describe the theoretical basics and the governing equations of the problem. In Section 3 we present the numerical procedure of a NURBS-based multi-step method and DQM, whose numerical results are discussed and compared in Section 4 for different mechanical, geometrical, and thermal parameters. The main conclusions of our work are, finally, summarized in Section 5.

2. Governing Equations

Let us describe the mathematical problem and its governing equations for a long FG cylindrical panel with an inner and outer piezoelectric layer. The laminated panel features an opening angle θ_0 , an inner radius R_i , and an outer radius R_o , whereby h_c is the FG layer thickness, h_p is the piezoelectric layer thickness, and for a total thickness $h = h_c + 2h_p$ (see Figure 1). A cylindrical coordinate system (r, θ, z) is chosen to identify the material points of the laminated panel in the undeformed configuration, as visible in Figure 1. The FG core layer is assumed to change gradually throughout the radial direction, namely, the mechanical properties vary continuously and smoothly from a ceramic-rich material (at the inner surface) to a metal-rich material (at the outer surface) according to a power law distribution. Thus, the effective material property P of the core is defined, accordingly, as

$$P(r) = P_c + (P_m - P_c) \left(\frac{r - R_i}{R_o - R_i} \right)^n \tag{1}$$

where n is a positive real number associated with the power law index (or the material property gradient index).

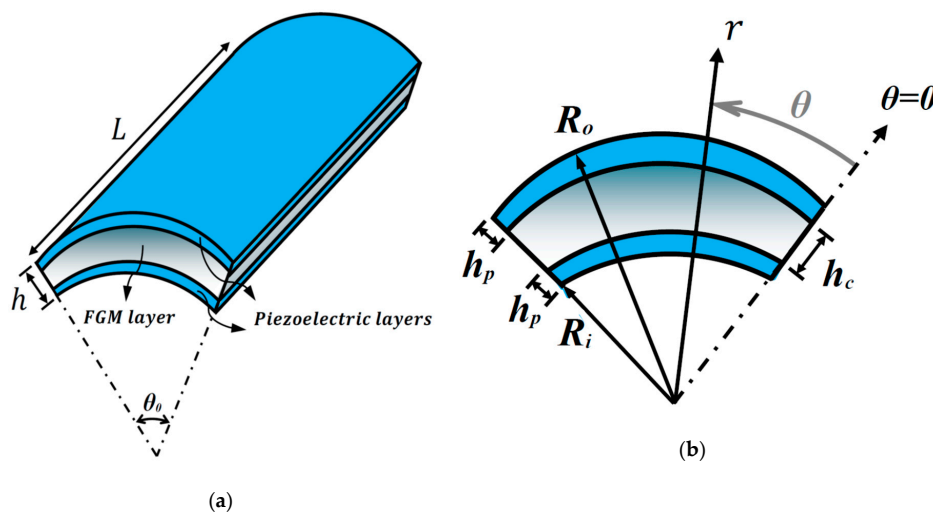


Figure 1. (a) and (b): Geometry of the FG cylindrical panels embedded in piezoelectric layers.

Long panels follow the plane strain assumptions, as employed thereafter. Accordingly, the linear constitutive relations for the core (i.e., the FG layer) and the piezoelectric layers take the following form, respectively [30]:

$$\begin{Bmatrix} \sigma_{rr}^c \\ \sigma_{\theta\theta}^c \\ \sigma_{r\theta}^c \end{Bmatrix} = \begin{bmatrix} C_{11}^c & C_{12}^c & 0 \\ C_{12}^c & C_{22}^c & 0 \\ 0 & 0 & C_{55}^c \end{bmatrix} \begin{Bmatrix} \frac{\partial u^c}{\partial r} - \alpha^c (\Delta T)^c \\ \frac{1}{r} \left(\frac{\partial v^c}{\partial \theta} + u^c \right) - \alpha^c (\Delta T)^c \\ \frac{1}{r} \left(\frac{\partial u^c}{\partial \theta} - v^c \right) + \frac{\partial v^c}{\partial r} \end{Bmatrix}, \tag{2a}$$

$$\begin{Bmatrix} \sigma_{rr}^p \\ \sigma_{\theta\theta}^p \\ \sigma_{r\theta}^p \end{Bmatrix} = \begin{bmatrix} C_{11}^p & C_{12}^p & 0 \\ C_{12}^p & C_{22}^p & 0 \\ 0 & 0 & C_{55}^p \end{bmatrix} \begin{Bmatrix} \frac{\partial u^p}{\partial r} - \alpha^p (\Delta T)^p \\ \frac{1}{r} \left(\frac{\partial v^p}{\partial \theta} + u^p \right) - \alpha^p (\Delta T)^p \\ \frac{1}{r} \left(\frac{\partial u^p}{\partial \theta} - v^p \right) + \frac{\partial v^p}{\partial r} \end{Bmatrix} - \begin{Bmatrix} 0 \\ 0 \\ e_4 E_\theta \end{Bmatrix}, \tag{2b}$$

$$\begin{Bmatrix} D_r \\ D_\theta \end{Bmatrix} = \begin{bmatrix} e_3 & e_2 & 0 \\ 0 & 0 & e_4 \end{bmatrix} \begin{Bmatrix} \frac{\partial u^c}{\partial r} \\ \frac{1}{r} \left(\frac{\partial v^c}{\partial \theta} + u^c \right) \\ \frac{1}{r} \left(\frac{\partial u^c}{\partial \theta} - v^c \right) + \frac{\partial v^c}{\partial r} \end{Bmatrix} + \begin{bmatrix} K_{33} & 0 \\ 0 & K_{22} \end{bmatrix} \begin{Bmatrix} E_r \\ E_\theta \end{Bmatrix} + \begin{Bmatrix} P_3 (\Delta T)^c \\ 0 \end{Bmatrix} \tag{2c}$$

where $(i, j = r, \theta)$ is the stress tensor components in the FG core ($e = c$) and piezoelectric layers ($e = p$); u and v are the displacement components at an arbitrary material point of the panel along the r and θ -directions, respectively; α denotes the thermal expansion coefficient; $(\Delta T)^e = T^e - T_0$ is the temperature variation; T_0 is the shell stress free temperature; C_{ij}^e ($i, j = 1, 2, 5$) is the material elastic coefficients of the core and piezoelectric layers; D_i and E_i ($i = r, \theta$) are the electric displacement and electric field in the i th direction, respectively; and e_i ($i = 2, 3, 4$), K_{ii} ($i = 2, 3$) and P_3 refer to the piezoelectric, dielectric, and pyroelectric constants, respectively.

The following relations are introduced between the electric field E_i and the electric potential ψ in piezoelectric layers:

$$E_r = -\frac{\partial \psi}{\partial r}, \tag{3a}$$

$$E_\theta = -\frac{\partial \psi}{r \partial \theta} \tag{3b}$$

The FG cylindrical panel is subjected to an initial temperature T_0 before the variation of the thermal boundary conditions at the two external surfaces occurs. Under the plane strain assumptions, the governing equations are independent of the axial coordinate variable z . Thus, for the FG core layer and piezoelectric layers, the linearized coupled energy balance equation according to the L-S thermoelasticity theory together with the equation of motion can be defined as [1].

Energy balance equation:

$$\frac{1}{r} \frac{\partial}{\partial r} \left(r k^e \frac{\partial T^e}{\partial r} \right) + \frac{1}{r^2} \frac{\partial}{\partial \theta} \left(k^e \frac{\partial T^e}{\partial \theta} \right) = \rho^e c^e \left(\frac{\partial T^e}{\partial t} + \tau_0^e \frac{\partial^2 T^e}{\partial t^2} \right) + \bar{\alpha}^e T_0 \left(\tau_0^e \frac{\partial^2}{\partial t^2} + \frac{\partial}{\partial t} \right) \left(\frac{\partial u^e}{\partial r} + \frac{u^e}{r} + \frac{\partial v^e}{r \partial \theta} \right). \tag{4}$$

Equations of motion:

$$\frac{\partial \sigma_{rr}^e}{\partial r} + \frac{\partial \sigma_{r\theta}^e}{r \partial \theta} + \frac{\sigma_{rr}^e - \sigma_{\theta\theta}^e}{r} = \rho^e \frac{\partial^2 u^e}{\partial t^2} \tag{5}$$

$$\frac{\partial \sigma_{r\theta}^e}{\partial r} + \frac{\partial \sigma_{\theta\theta}^e}{r \partial \theta} + \frac{2\sigma_{r\theta}^e}{r} = \rho^e \frac{\partial^2 v^e}{\partial t^2} \tag{6}$$

where $\bar{\alpha}^e = \alpha^e (3\lambda^e + 2\mu^e)$, λ^e and μ^e are the Lamé constants of the layers ($e = p, c$); τ_0^e ($e = p, c$) is the relaxation time of the L-S theory, and t is the time.

Moreover, the piezoelectric layers are governed by the following electroelastic equation:

$$\frac{\partial D_r}{\partial r} + \frac{D_r}{r} + \frac{\partial D_\theta}{r \partial \theta} = 0. \tag{7}$$

Among different possibilities of assuming the thermal boundary conditions of the panel, in the present work we consider a drastic variation for the transient temperature (at the inner surface) and for the convection heat transfer (at the outer surface). In detail,

at

$$r = R_i: T^p = T_i \left(1 - e^{-t/t_0} \right) \tag{8a}$$

at

$$r = R_o: -k^p \frac{\partial T^p}{\partial r} = \hat{h}_c (T^p - T_\infty) \tag{8b}$$

where T_i is the temperature of the inner surface over a long period of time (i.e., $t \gg t_0$), t_0 is a time constant, T_∞ is the ambient temperature, and \hat{h}_c denotes the convective heat transfer coefficient.

By neglecting the heat transfer from the straight edges of the panel (i.e., $\theta = 0$ and $\theta = \theta_0$), the corresponding thermal condition becomes

$$\frac{\partial T^e}{\partial \theta} = 0 \quad e = p, c \tag{9}$$

The mechanical boundary conditions at the inner and outer surfaces of the panels ($r = R_i, R_o$) are defined as follows:

$$\sigma_{rr}^p = 0 \text{ or } C_{11}^p \frac{\partial u^p}{\partial r} + \frac{C_{12}^p}{r} \left(\frac{\partial v^p}{\partial \theta} + u^p \right) = (C_{11}^p + C_{12}^p) \alpha^p (T^p - T_0) \tag{10a}$$

$$\sigma_{r\theta}^p = 0 \text{ or } C_{55}^p \left[\frac{1}{r} \left(\frac{\partial u^p}{\partial \theta} - v^p \right) + \frac{\partial v^p}{\partial r} \right] = e_4 E_\theta \tag{10b}$$

Moreover, the following thermal and mechanical compatibility conditions are enforced at the interface between the FG core and piezoelectric layers of the panel (i.e., $r = R_i + h_p$, $r = R_o - h_p$), respectively.

$$T^p(r, t) = T^c(r, t), \tag{11a}$$

$$k^p \frac{\partial T^p(r, t)}{\partial r} = k^c \frac{\partial T^c(r, t)}{\partial r} \tag{11b}$$

$$u^p(r, t) = u^c(r, t), v^p(r, t) = v^c(r, t) \tag{12a}$$

$$C_{11}^p \frac{\partial u^p}{\partial r} + \frac{C_{12}^p}{r} \left(\frac{\partial v^p}{\partial \theta} + u^p \right) - (C_{11}^p + C_{12}^p) \alpha^p (T^p - T_0) = C_{11}^c \frac{\partial u^c}{\partial r} + \frac{C_{12}^c}{r} \left(\frac{\partial v^c}{\partial \theta} + u^c \right) - (C_{11}^c + C_{12}^c) \alpha^c (T^c - T_0) \tag{12b}$$

$$C_{55}^p \left[\frac{1}{r} \left(\frac{\partial u^p}{\partial \theta} - v^p \right) + \frac{\partial v^p}{\partial r} \right] - e_4 E_\theta = C_{55}^c \left[\frac{1}{r} \left(\frac{\partial u^c}{\partial \theta} - v^c \right) + \frac{\partial v^c}{\partial r} \right] \tag{12c}$$

In this study, clamped boundary conditions are assumed at the edges $\theta = 0$ and $\theta = \theta_0$, namely,

$$u^e = 0, v^e = 0 \tag{13a}$$

$$e = p, c \tag{13b}$$

whereby the initial thermal and mechanical conditions are assumed, respectively, as follows:

$$T^e(r, 0) = T_0 \tag{14a}$$

$$\left. \frac{\partial T^e(r, t)}{\partial t} \right|_{t=0} = 0 \tag{14b}$$

$$u^e(r, 0) = 0 \tag{15a}$$

$$v^e(r, 0) = 0 \tag{15b}$$

$$\left. \frac{\partial u^e(r, t)}{\partial t} \right|_{t=0} = 0. \tag{15c}$$

$$\left. \frac{\partial v^e(r, t)}{\partial t} \right|_{t=0} = 0 \tag{15d}$$

3. Solution Procedure

The analytical solution of the abovementioned governing equations of the problem with variable coefficients is clearly difficult and cumbersome, whereas a semi-analytical or numerical method should

be more convenient and suitable for use. Due to the computational efficiency and accuracy of the DQM demonstrated in the literature for different heat transfer and structural problems [11,20,36,43–52], we combined this method with the NURBS-based multi-step method in the current work to discretize the governing equations in the spatial and time domains, respectively. Based on the DQM, the FG core and piezoelectric layers are discretized into a set of N_ξ^e ($e = c, p$) and N_θ grid points along the r - and θ -directions, respectively. In this regard, the Gauss–Lobatto–Chebyshev grid generation rule is employed [11,20,36,43–52]. Thus, the spatial derivatives involved in the differential equations are discretized together with the corresponding thermo-mechanical boundaries and compatibility conditions at the interface between the core and piezoelectric layers. For the sake of brevity, we describe only the discretized form for the of energy balance from Equation (4), as also repeated for all the other equations of the problem.

$$\begin{aligned} \rho_i^e c_i^e \left[\frac{dT_{ij}^e}{dt} + (\tau_0^e)_i \frac{d^2 T_{ij}^e}{dt^2} \right] + \bar{\alpha}_i^e T_0 \left[(\tau_0^e)_i \frac{\partial^2}{\partial t^2} + \frac{\partial}{\partial t} \right] & \left(\sum_{m=1}^{N_\xi^e} A_{im}^\xi u_{mj}^e + \frac{u_{ij}^e}{r_{ij}} + \frac{1}{r_{ij}} \sum_{n=1}^{N_\theta} A_{jn}^\theta v_{in}^e \right) \\ & = k_i^e \sum_{m=1}^{N_\xi^e} B_{im}^\xi T_{mj}^e + \frac{2k_i^e}{r_i} \sum_{m=1}^{N_\xi^e} A_{im}^\xi T_{mj}^e + \frac{k_i^e}{r_i^2} \sum_{n=1}^{N_\theta} A_{jn}^\theta T_{in}^e \end{aligned} \tag{16}$$

where $e = c, p$; $i = 2, \dots, \hat{N}_\xi^e (= N_\xi^e - 1)$; $j = 2, \dots, \hat{N}_\theta (= N_\theta - 1)$; and A_{ij}^β and B_{ij}^β ($\beta = r, \theta$) represent the first- and second-order weighting coefficients for the β -direction ($\beta = r, \theta$), respectively, which is computed here through the Lagrange polynomials.

Once the DQM discretization procedure is completed, we get the following system of ordinary differential equations (ODEs) in the time domain:

$$\mathbf{M} \frac{d^2 \mathbf{D}}{dt^2} + \mathbf{C} \frac{d\mathbf{D}}{dt} + \mathbf{K} \mathbf{D} = \mathbf{f}(t) \tag{17}$$

where \mathbf{D} is the vector of degrees of freedom (i.e., temperature and displacement components at grid points); \mathbf{M} , \mathbf{C} , and \mathbf{K} represent the mass, thermoelastic damping, and stiffness matrices, respectively; and $\mathbf{f}(t)$ is the load vector.

A NURBS-based multi-step method [37] is here adopted to solve the system of ODE (17) according to the initial conditions. The higher performance of this technique with respect to the conventional finite difference-based schemes, such as the Newmark’s time integration scheme, has been recently demonstrated by Heydarpour et al. [37]. To apply this method, the second-order system of Equation (17) is transformed into a first-order one, as follows:

$$\begin{cases} \frac{d\mathbf{\Psi}_1}{dt} = \mathbf{\Psi}_2 & (18a) \\ \mathbf{M} \frac{d\mathbf{\Psi}_2}{dt} + \mathbf{C}\mathbf{\Psi}_2 + \mathbf{K}\mathbf{\Psi}_1 = \mathbf{f}(t) & (18b) \end{cases}$$

where $\mathbf{\Psi}_1 = \mathbf{D}$ and $\mathbf{\Psi}_2 = \frac{d\mathbf{D}}{dt}$. Based on the present approach, a different multi-step scheme can be generated by changing the order and/or the weighting coefficients (w_i) of the NURBS curves. In this study, a four-step scheme [37] with the weight coefficients $w_1 = 0.001$, $w_2 = 0.001$, $w_3 = 2$ and $w_4 = 3$ is considered to solve Equation (18a,b), the discretized form of which can be expressed as follows:

$$\mathbf{\Psi}_{1,n+1} = \mathbf{\Psi}_{1,n} + \Delta t (1.50002585 \mathbf{\Psi}_{2,n} - 0.50005291 \mathbf{\Psi}_{2,n-1} + 0.00002827 \mathbf{\Psi}_{2,n-2} - 0.00000120 \mathbf{\Psi}_{2,n-3}) \tag{19}$$

$$\mathbf{\Psi}_{2,n+1} = \mathbf{\Psi}_{2,n} + \Delta t (1.50002585 \hat{\mathbf{\Psi}}_n - 0.50005291 \hat{\mathbf{\Psi}}_{n-1} + 0.00002827 \hat{\mathbf{\Psi}}_{n-2} - 0.00000120 \hat{\mathbf{\Psi}}_{n-3}) \tag{20}$$

where Δt is the time step size, and

$$\hat{\mathbf{\Psi}} = \mathbf{M}^{-1} (-\mathbf{C}\mathbf{\Psi}_2 - \mathbf{K}\mathbf{\Psi}_1 + \mathbf{f}(t)) \tag{21}$$

The solution process starts with the initial conditions to determine the unknown field variables at the first four points. Subsequently, by employing the multi-step scheme, Equation (18a,b) is converted into a system of linear algebraic equations whose solution is related to the field variables at the end of each time step. By repeating the process, we are able to determine the displacement components and temperature at the grid points of FG cylindrical panel.

4. Numerical Results

We start this section with a validation of the proposed approach, which is followed by a parametric study that investigates the sensitivity of the thermoelastic response of the panel to the mechanical, thermal, or geometrical input parameters. Unless otherwise mentioned, we consider Ti-6Al-4V and ZrO₂ in the numerical examples to be the metal and ceramic phases, respectively (Table 1), and we introduce the following dimensionless parameters

$$F_o = \frac{t\hat{\alpha}_m}{h^2}, \tag{22a}$$

$$\tau = \frac{\tau_0\hat{\alpha}_m}{h^2}, \tag{22b}$$

$$T^* = \frac{T - T_\infty}{T_\infty}, \tag{22c}$$

$$U = \frac{u}{(1 - \nu_c)\alpha_c T_\infty R_m}, \tag{22d}$$

$$\xi = \frac{r - R_i}{R_o - R_i}, \tag{22e}$$

$$\Sigma_{ii} = \frac{(1 + \nu_c)}{E_c \alpha_c T_\infty} \sigma_{ii} \tag{22f}$$

with

$$i = r, \theta. \tag{22g}$$

where $\hat{\alpha}_m (= k_m / \rho_m c_m)$ is the thermal diffusivity of the metal, and the following geometry and physical parameters are assumed: $R_m = 1$ (m), $h = 0.35$ m, $T_0 = T_\infty = 300$ K, $T_i = 800$ K, $\hat{h}_c = 10$ W/m²K, $t_0 = 2$ s. The piezoelectric layers are made of lead zirconate titanate (PZT-4) with the mechanical properties given in Table 2, in accordance with [30].

As a first example, we compare the CPU time necessary for a thermoelastic study of a FG cylindrical panel, as provided by a NURBS-based multi-step time integration scheme and a Newmark's method.

Table 3 gathers the convergence results for the dimensionless displacement, hoop stress, and temperature at point $\xi = 0.5$, $\theta = 0.5\theta_0$ versus the number of time steps N_t . As visible in Table 3, a NURBS-based multi-step approach requires a lower CPU time compared to a classical Newmark's method. Accordingly, Figures 2 and 3 depict the convergence results from a transient thermoelastic study of FG cylindrical panels with a piezoelectric layer under a thermal loading condition. In these figures, the variations along the thickness direction of the dimensionless temperature, radial displacement, and hoop stress components are reported versus the DQ number of grid points throughout the thickness ($N_\xi^e = N_\xi$, $e = c, p$) and circumferential direction (N_θ). It is worth observing that nine grid points in the radial direction per layer (i.e., $N_\xi = 9$) and eleven grid points in the circumferential direction yielded acceptable results. Hence, the values of $N_\xi = 9$, $N_\theta = 11$, and $N_t = 300$ are assumed hereafter within the numerical investigation.

Table 1. Material properties of ceramic (ZrO₂) and metal (Ti-6Al-4V) [11].

Material	Ti-6Al-4V	ZrO ₂
k [W/mK]	18.1	2.036
ρ [kg/m ³]	4410	5600
C [J/kgK]	808.3	615.6
E [GPa]	66.2	117
α [1/K]	10.3×10^{-6}	7.11×10^{-6}
ν	0.322	0.322

Table 2. Material properties of the lead zirconate titanate (PZT-4) [30].

	115	d_1 (coul/N)	-3.92×10^{-12}
C_{22} [GPa]	139	V_p	0.31
C_{55} [GPa]	25.6	E_p [GPa]	63
C_{12} [GPa]	74	ρ_p [kg/m ³]	7500
e_2 [coul/m ²]	-5.2	C_p [J/kgK]	350
e_3 [coul/m ²]	15.1	α_{pr} [1/K]	2.62×10^{-6}
e_4 [coul/m ²]	12.7	$\alpha_{p\theta}$ [1/K]	1.97×10^{-6}
μ_2 [nF/m]	6.5	k_{pr} [W/mK]	1.5
μ_3 [nF/m]	5.6	$k_{p\theta}$ [W/mK]	2.1
P_3 (coul/m ² K)	5.4×10^{-5}		

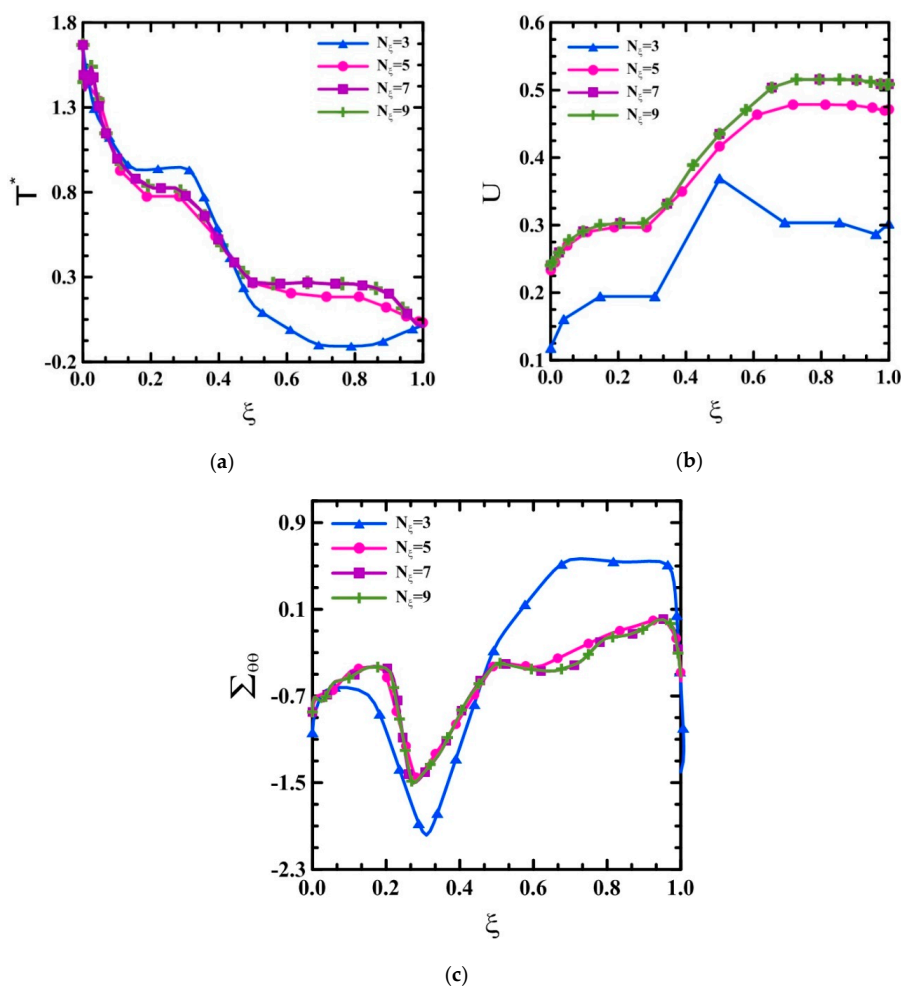


Figure 2. (a–c): Parametric analysis of the thermoelastic field variables vs. the number of grid points ($n = 1, h_c/h_p = 5, N_\theta = 11, N_t = 300, \theta_0 = 75^\circ, \theta = 0.5\theta_0, \psi = 0.03, F_0 = 0.8, \tau = 0.2$).

Table 3. Comparison between a NURBS-based multi-step technique and the Newmark’s scheme ($n = 1, h_c/h_p = 5, \theta_0 = 75^\circ, \psi = 0.03, \xi = 0.5, \theta = 0.5\theta_0, F_0 = 0.8, \tau = 0.1$).

NURBS-Based Multi-Step Method					Newmark’s Method (Galerkin Scheme)			
N_t	T^*	U	$\Sigma_{\theta\theta}$	CPU Time (s)	T^*	U	$\Sigma_{\theta\theta}$	CPU Time (s)
10	0.523	0.704	-0.836	0.0024	0.311	0.456	-0.425	9.400
25	0.449	0.581	-0.732	0.0196	0.340	0.448	-0.616	18.106
50	0.405	0.549	-0.584	0.0263	0.339	0.473	-0.483	37.406
75	0.367	0.516	-0.529	0.0339	0.340	0.475	-0.486	53.471
100	0.352	0.489	-0.506	0.0408	0.341	0.475	-0.488	69.603
125	0.346	0.481	-0.497	0.0452	0.342	0.476	-0.490	81.531
200	0.342	0.476	-0.491	0.0584	0.342	0.476	-0.490	146.73
300	0.342	0.475	-0.489	0.0660	0.342	0.476	-0.490	343.89

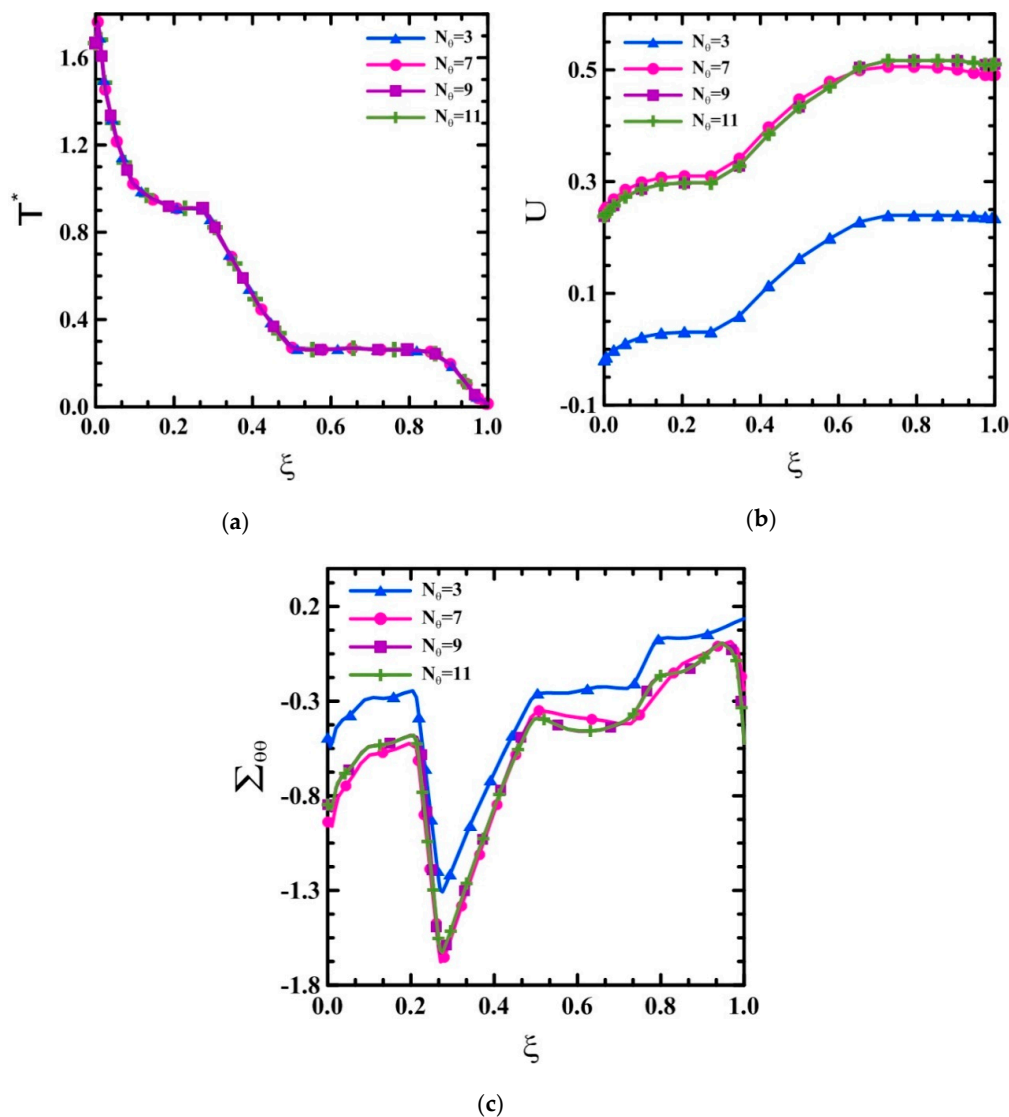


Figure 3. (a–c): Parametric analysis of the thermoelastic field variables vs. the number of grid points ($n = 1, h_c/h_p = 5, N_\xi = 9, N_t = 300, \theta_0 = 75^\circ, \theta = 0.5\theta_0, \psi = 0.03, F_0 = 0.8, \tau = 0.2$).

For validation purposes, we analyzed the FG hollow cylindrical shells under a thermal loading, as a limit case of cylindrical panels. Therefore, by setting $\theta_0 = 2\pi$ and enforcing the geometric and physical compatibility conditions at $\theta = 0$ and $\theta = \theta_0 = 2\pi$, a FG cylindrical panel reverted to a

cylindrical shell. This case study is here selected in agreement with [53], where a semi-analytical finite element method was applied for the analysis of FG cylindrical shells under the following thermal boundary and initial conditions:

at

$$r = R_i : T(r, z, t) = T_0(1 - e^{-0.5t}) \tag{23a}$$

$$r = R_o : k \frac{\partial T}{\partial r} + h_c T = 0 \tag{23b}$$

at

$$z = 0, L : \tag{23c}$$

$$T(r, z, t) = 0 \tag{23d}$$

$$T(r, z, 0) = 0, \tag{23e}$$

$$\left. \frac{\partial T(r, z, t)}{\partial t} \right|_{t=0} = 0. \tag{23f}$$

As far as the material properties are concerned, they vary throughout the shell thickness from a ceramic-rich material, at the inner surface, to a metal-rich material, at the outer surface, in accordance with Equation (1). The metal and ceramic mechanical properties are listed in Table 4. The dimensionless temperature and displacement distributions across the shell thickness are depicted in Figure 4 for a varying material graded index n , where the accuracy of the proposed method against the uncoupled theory proposed in [53] is confirmed by the very good agreement between results.

Table 4. Material properties of ceramic (Zirconia) and metal (steel) [53].

Material	Zirconia	Steel
k [W/cm °C]	2.09	20
ρ [kg/m ³]	5700	8166
C_v [J/kg °C]	531.9	325.35
E [MPa]	168.06	207.79
α [1/°C]	2.3×10^{-4}	1.5×10^{-5}
ν	0.298	0.3178

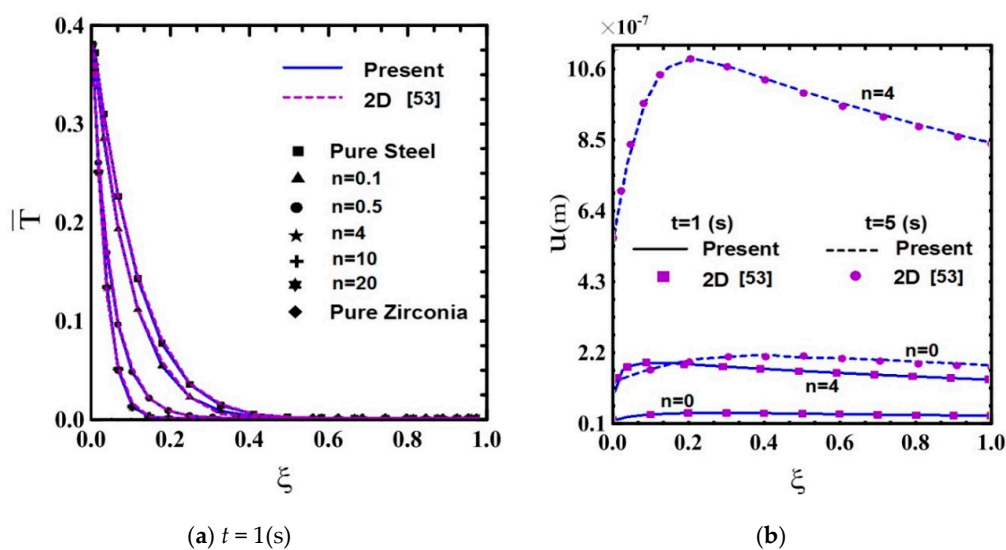


Figure 4. (a,b): Transient dimensionless temperature distributions and displacement field across the thickness of an FG hollow cylinder subjected to a prescribed temperature at its inner surface ($R_i = 4\text{cm}$, $R_o = 6\text{cm}$, $L = 20\text{cm}$, $\bar{T} = T/T_0$, $\eta = 0.5$).

The effect of the material gradient index n on the through-the-thickness variation and time histories of the thermoelastic field variables is plotted in Figures 5 and 6 for FG cylindrical panels with piezoelectric layers under a thermal shock at the inner surface. The heat wave front can easily be seen in Figures 5a and 6a, where panels with a pure metal core (i.e., $n = 0$) feature a higher value of heat wave speed compared to the ones with nonhomogeneous cores (i.e., $n \neq 0$). In addition, the heat wave speed increases by increasing the metal content, or equivalently with a decreasing value of n .

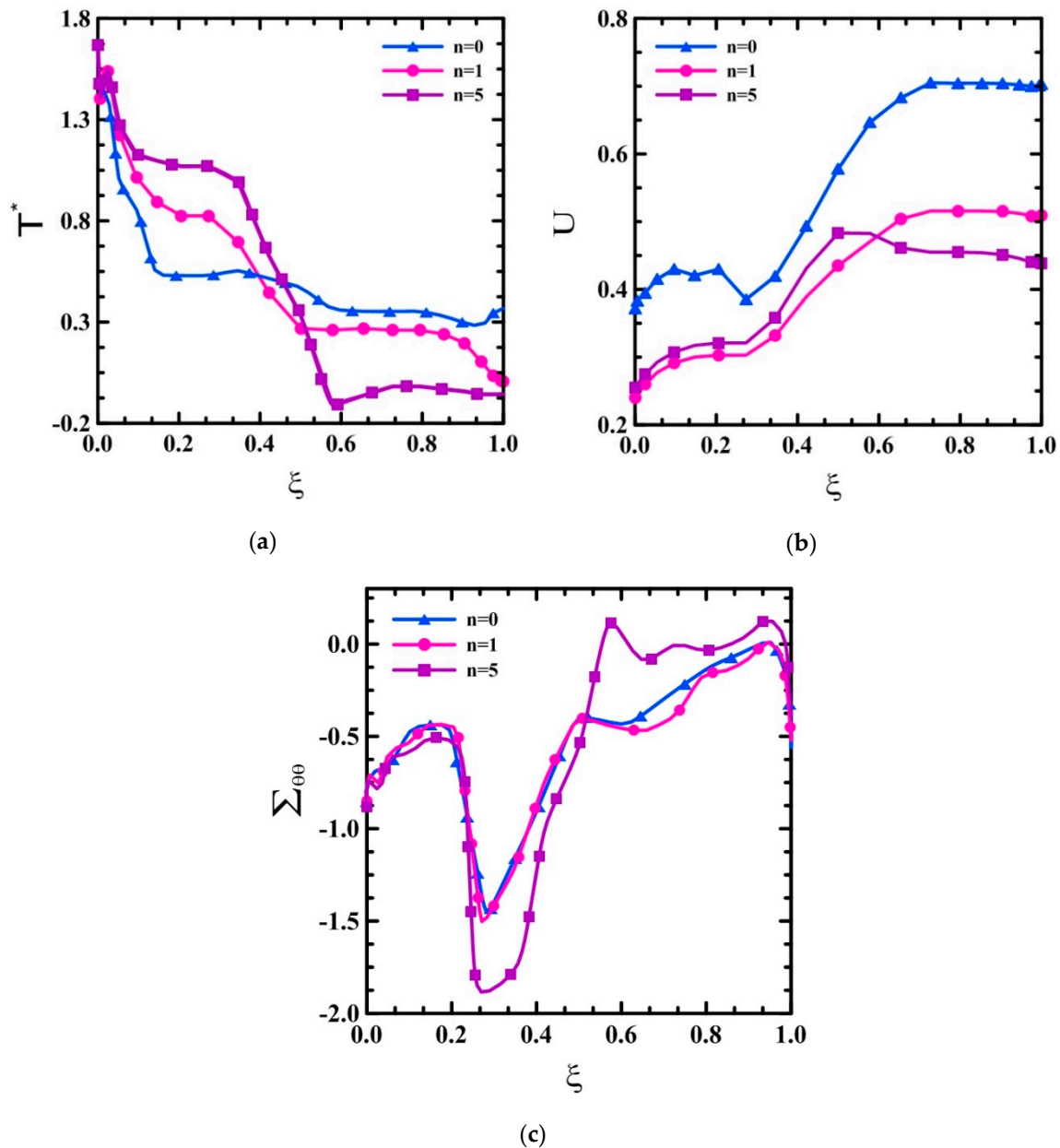


Figure 5. (a–c): Effect of the material gradient index n on the distribution of the thermoelastic field variables through the radial direction for the FG cylindrical panels with piezoelectric layers ($h_c/h_p = 5$, $\theta_0 = 75^\circ$, $\psi = 0.03$, $\theta = 0.5\theta_0$, $F_0 = 0.8$, $\tau = 0.2$).

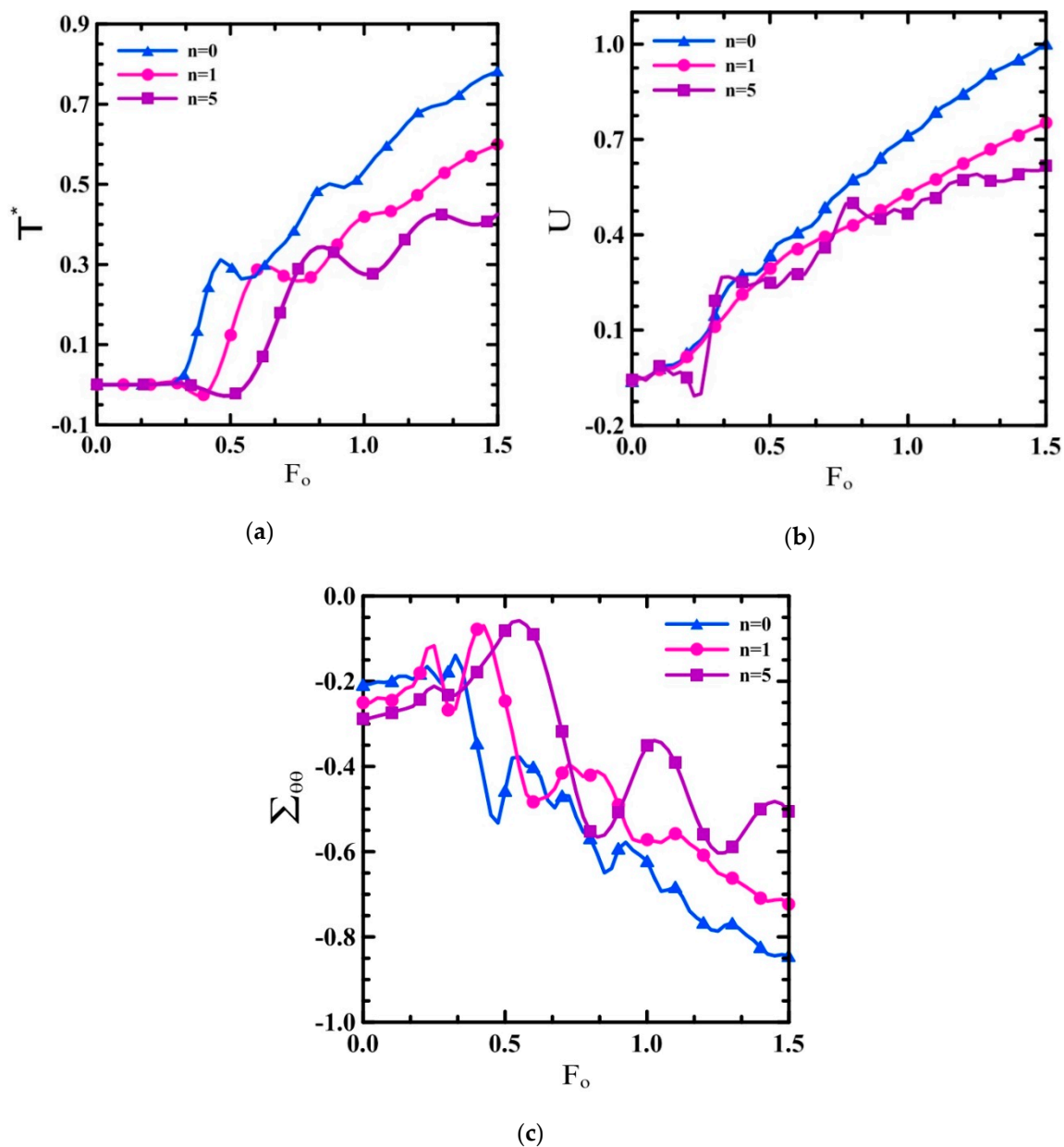


Figure 6. (a–c): Effect of the material gradient index n on the time histories of the thermoelastic field variables for the FG cylindrical panels with piezoelectric layers ($h_c/h_p = 5$, $\theta_0 = 75^\circ$, $\psi = 0.03$, $\xi = 0.5$, $\theta = 0.5\theta_0$, $\tau = 0.2$).

Figures 7 and 8 also plot the effect of the dimensionless relaxation time τ on the thermoelastic response of FG cylindrical panels with piezoelectric layers, revealing the through-the-thickness variations and time histories of the thermoelastic field variables of a material point ($\xi = 0.5$, $\theta = 0.5\theta_0$), respectively. Based on Figures 7 and 8, it is clear that the use of either a classical thermoelasticity theory (i.e., $\tau = 0$) or the L-S theory (i.e., the case with $\tau \neq 0$) leads to significant differences in the numerical results, evaluated here in terms of temperature, radial displacement, and hoop stress. Moreover, the oscillating behavior of the temperature time histories for $\tau \neq 0$, (i.e., for a non-Fourier heat conduction law) plotted in Figure 8a, indicates the necessity of using the L-S theory for thermal shock loading problems.

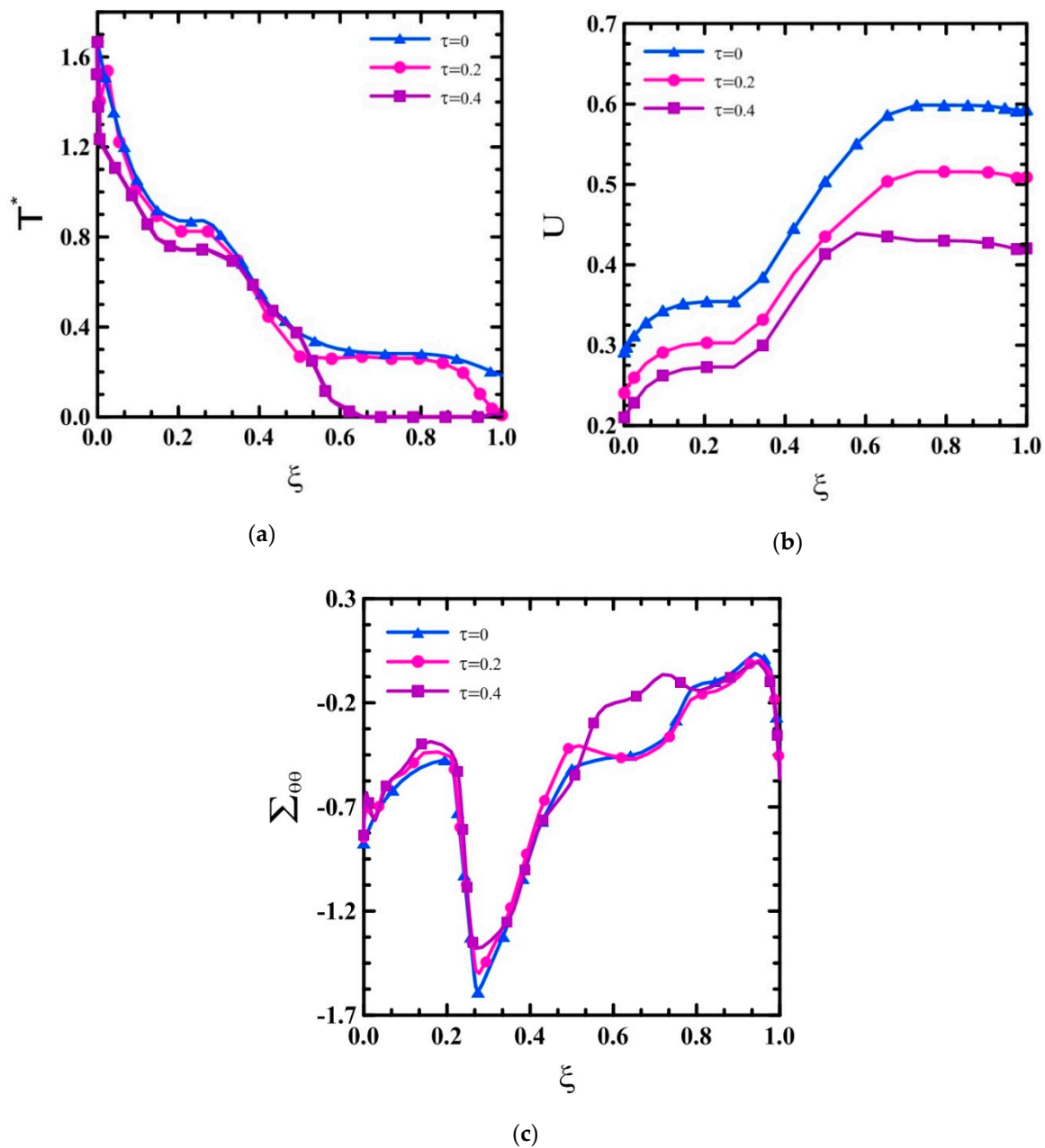


Figure 7. (a–c): Effect of the relaxation time on the distribution of the thermoelastic field variables through the radial direction for the FG cylindrical panels with piezoelectric layers ($p = 1, h_c/h_p = 5, \theta_0 = 75^\circ, \psi = 0.03, \theta = 0.5\theta_0, F_0 = 0.8$).

The through-the-thickness heat wave propagation and the resulting variations in the mechanical field variables of the FG cylindrical panels with piezoelectric layers are shown in Figure 9a–c for different non-dimensional time levels F_0 . The results clearly demonstrate that the model can simulate thermoelastic wave propagation in multilayer panels. It is worth observing that the temperature and the radial displacement increase with an increasing dimensionless time F_0 .

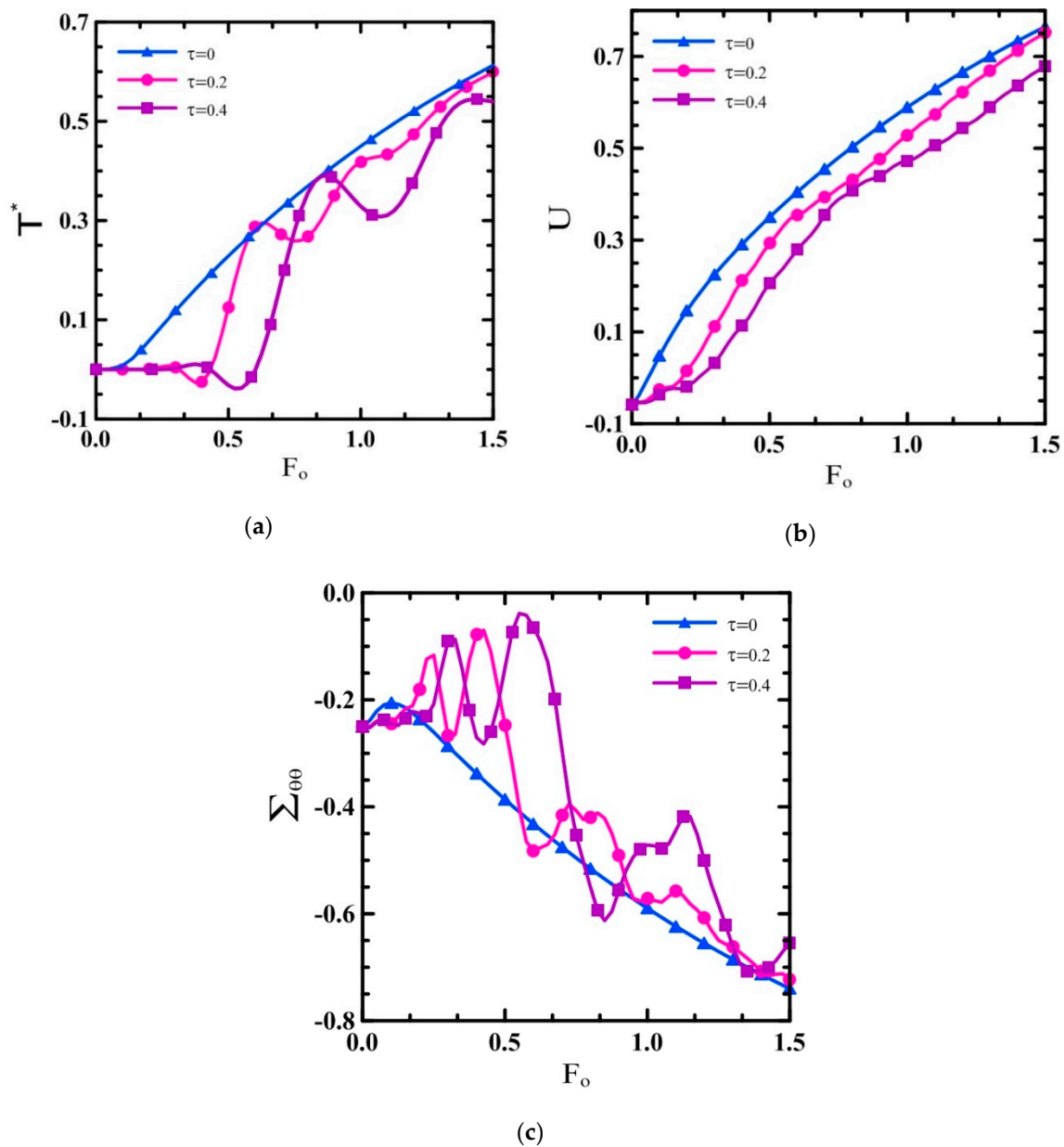


Figure 8. (a–c): Time histories of the thermoelastic field variables against the relaxation time ($n = 1, h_c/h_p = 5, \theta_0 = 75^\circ, \psi = 0.03, \xi = 0.5, \theta = 0.5\theta_0$).

In Figure 10, the effect of the core thickness-to-piezoelectric thickness ratio h_c/h_p on the thermoelastic behavior of FG cylindrical panels is described, where an increased value of h_c/h_p yields a general increase of all the field variables. A further systematic study considers the effect of the panel opening angle θ_0 on the through-the-thickness variation of the dimensionless thermoelastic field variables, as depicted in Figure 11a–c. As expected, by increasing θ_0 , the radial displacement increases, and the hoop stress component decreases, although the maximum values of the field variables involve the same locations of the panel independently of θ_0 . Furthermore, in Figure 12a–c, we evaluate the effect of the opening angle θ_0 on the time histories for all thermoelastic field variables while considering the material points $\xi = 0.5$ and $\theta = 0.5\theta_0$. Also visible in Figures 11a and 12a, the distribution and time histories of the temperature seem to be unaffected by a variation in θ_0 .

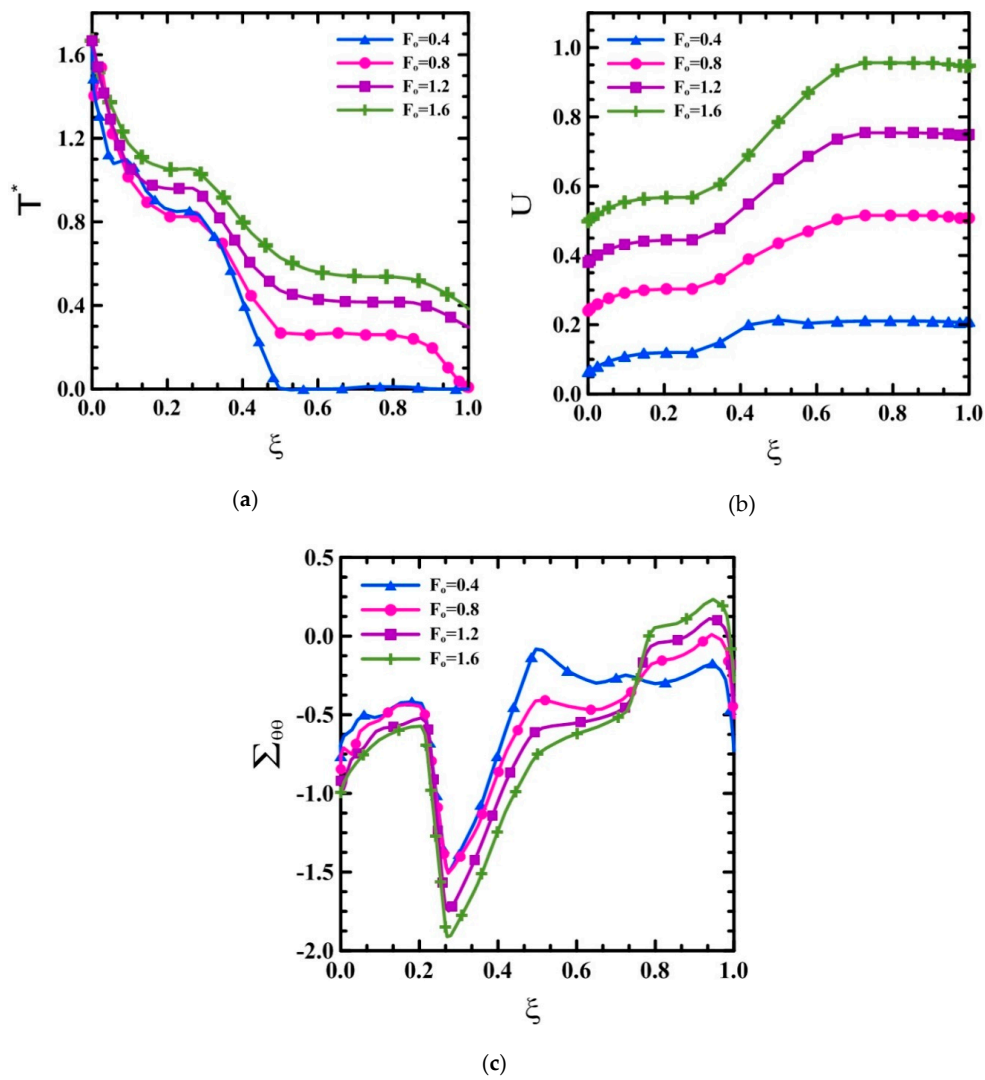


Figure 9. (a–c): Effects of different time levels on the distribution of the thermoelastic field variables through the radial direction ($n = 1, h_c/h_p = 5, \theta_0 = 75^\circ, \theta = 0.5\theta_0, \psi = 0.03, \tau = 0.2$).

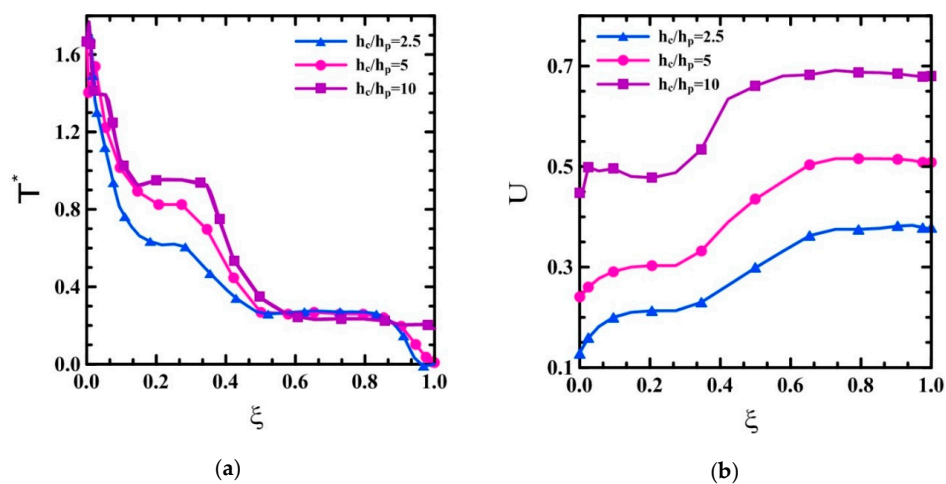
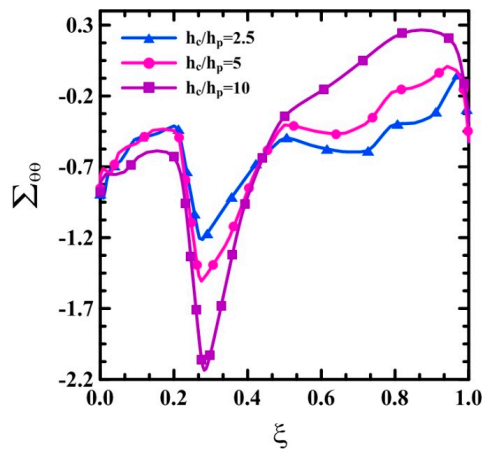
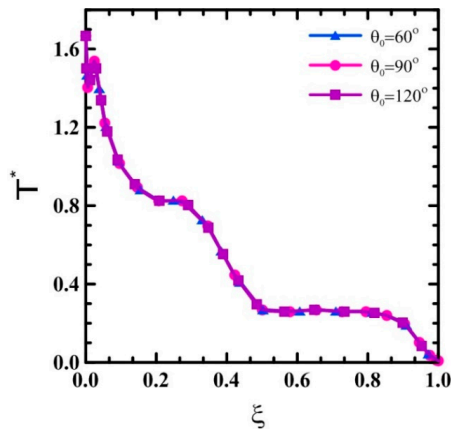


Figure 10. Cont.

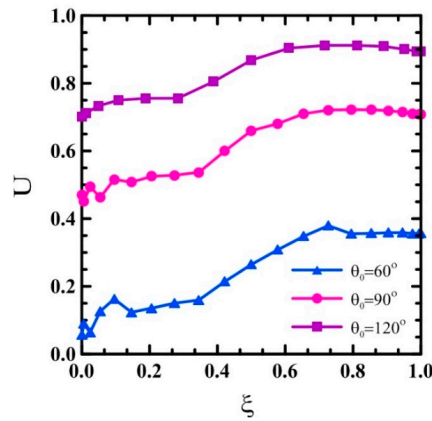


(c)

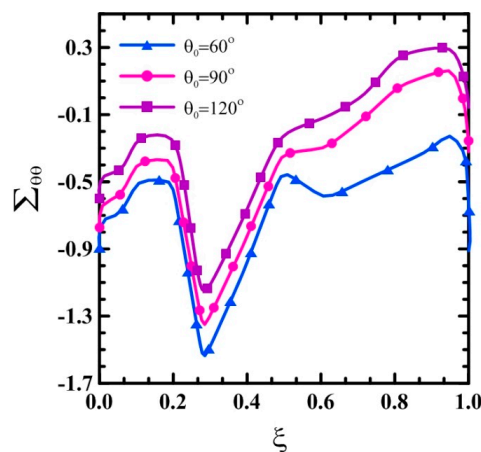
Figure 10. (a–c): Effect of the core thickness-to-piezoelectric thickness ratio h_c/h_p on the distribution of the thermoelastic field variables through the radial direction ($n = 1$, $\theta_0 = 75^\circ$, $\theta = 0.5\theta_0$, $\psi = 0.03$, $F_0 = 0.8$, $\tau = 0.2$).



(a)



(b)



(c)

Figure 11. (a–c): Effect of the opening angle θ_0 on the distribution of the thermoelastic field variables in the radial direction ($n = 1$, $h_c/h_p = 5$, $\theta = 0.5\theta_0$, $\psi = 0.03$, $F_0 = 0.8$, $\tau = 0.2$).

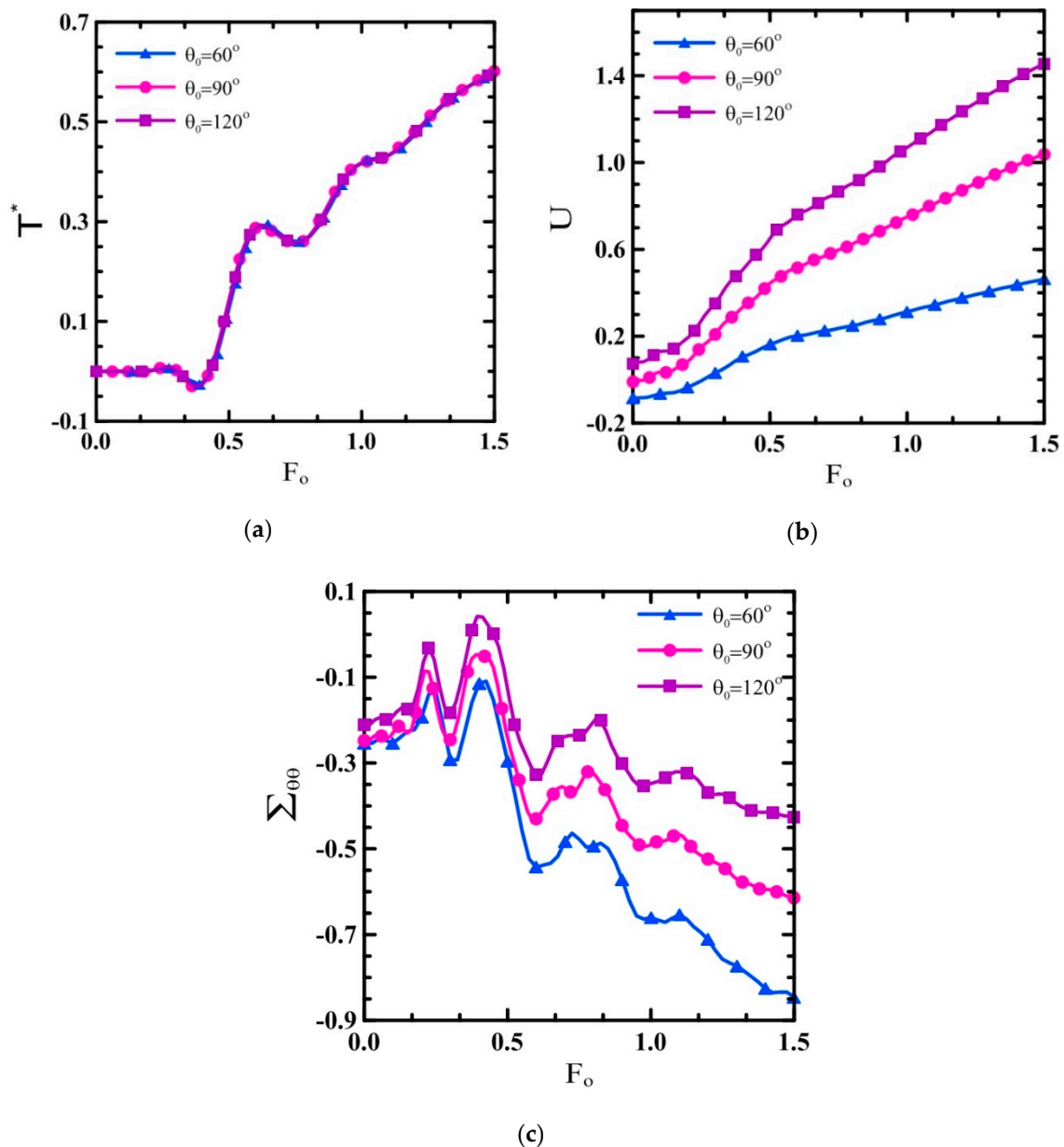


Figure 12. (a–c): Time histories of the thermoelastic field variables against the opening angle θ_0 , ($n = 1, h_c/h_p = 5, \xi = 0.5, \theta = 0.5\theta_0, \psi = 0.03, \tau = 0.2$).

In the last parametric study, we checked the sensitivity of the thermoelastic response of FG cylindrical panels with piezoelectric layers to varying external electrical voltages (Figures 13 and 14). More specifically, we evaluated the through-the-thickness variations and time histories of the dimensionless thermoelastic field variables for three different values of external electrical voltage $\psi = 0; 0.03; 0.06$. As clearly visible in Figures 13a and 14a, an increase in the external electrical voltage did not affect the temperature variations, but it led to an overall decrease in radial displacement and an increase of the hoop stress component.

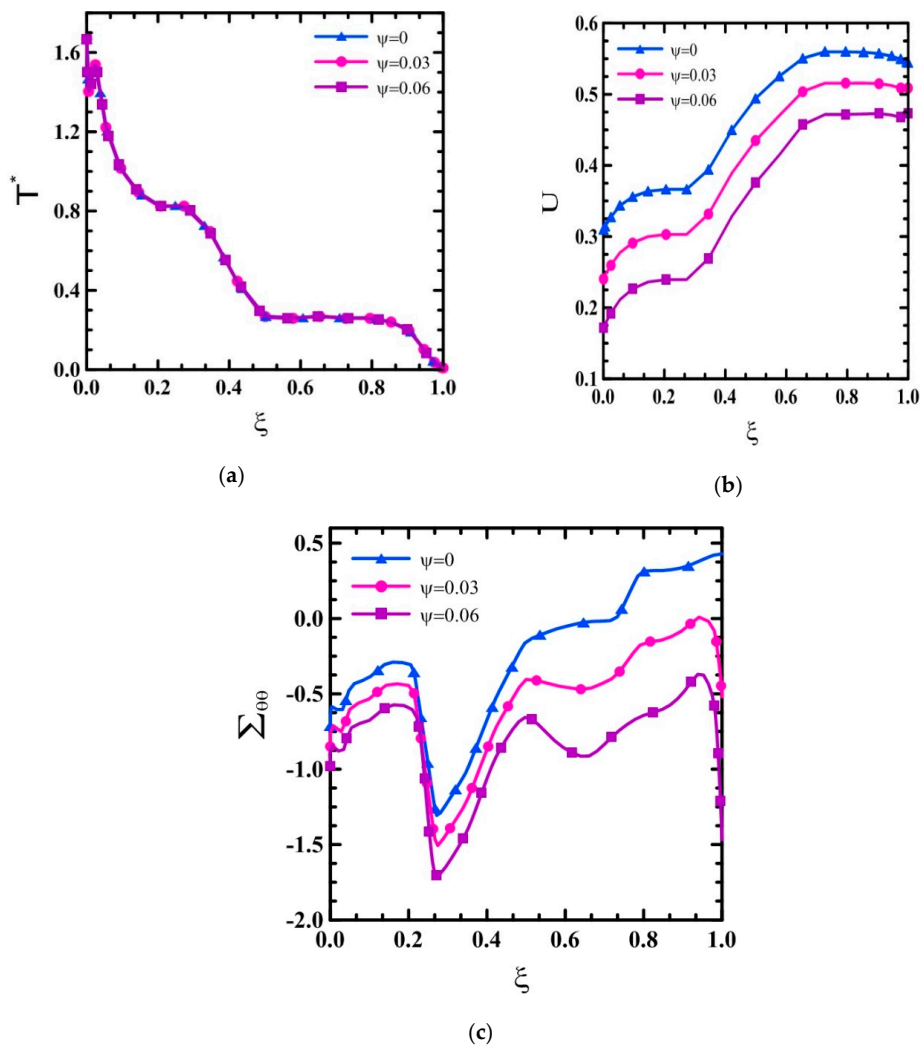


Figure 13. (a–c): Effect of the external electrical voltage ψ on the distribution of the thermoelastic field variables in the radial direction ($n = 1, h_c/h_p = 5, \theta = 0.5\theta_0, F_0 = 0.8, \tau = 0.2$).

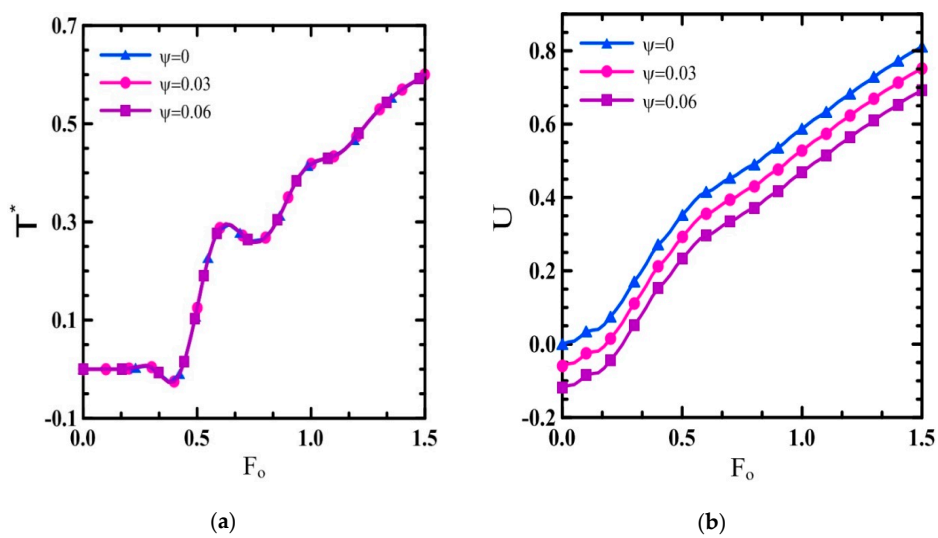
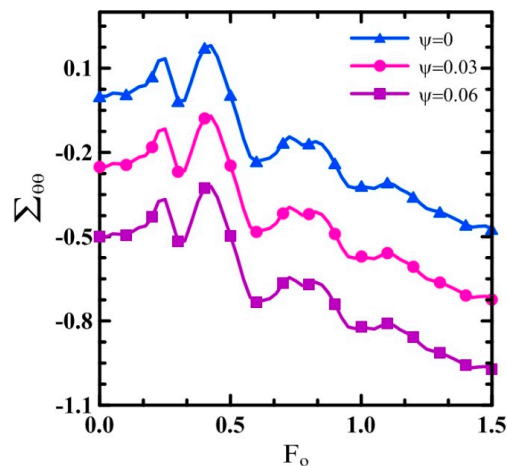


Figure 14. Cont.



(c)

Figure 14. (a–c): Time histories of the thermoelastic field variables against the external electrical voltage ($n = 1$, $h_c/h_p = 5$, $\theta_0 = 75^\circ$, $\xi = 0.5$, $\theta = 0.5\theta_0$, $\tau = 0.2$).

5. Conclusions

In this paper, we have proposed a coupled thermoelasticity theory of Lord–Shulman and Maxwell’s equation, to examine thermoelastic wave propagation for FG cylindrical panels with inner and outer surfaces bonded by piezoelectric layers, and subjected the panels to a thermal shock loading. The coupled governing equations of the problem have been solved using a computationally efficient and accurate numerical hybrid method built upon a discrete LW-DQM method and a NURBS-based multi-step time integration scheme. The geometric and physical compatibility conditions have been enforced exactly at the interfacial layers. The model is able to accurately simulate the variations of the field variables throughout the thickness, as demonstrated by the fast rate of convergence of the numerical results. A wide parametric study has considered the effects of the material graded index, piezoelectric layer thickness, external electrical voltage, and opening angle on the thermoelastic behavior of FG cylindrical panels, while providing the following promising conclusions for practical applications:

- The model can simulate thermoelastic wave propagation in multilayer panels.
- An increased material gradient index n decreases the heat wave speed.
- The classical thermoelasticity theory based on a null value of relaxation time is unable to accurately predict the thermoelastic behavior of laminated panels under a thermal shock loading.
- An increased core thickness-to-piezoelectric thickness ratio h_c/h_p yields an increased value of all the thermoelastic field variables.
- An increased opening angle of the panel θ_0 increases the radial displacement and decreases the hoop stress component.
- The location of the maximum values for the hoop stress is almost independent of the geometrical opening angle θ_0 .
- The opening angle θ_0 does not allow any sensitive variation in the distribution and time histories of the temperature.
- An increased external electrical voltage decreases the radial displacement and increases the hoop stress component without affecting the temperature variation.

Author Contributions: Conceptualization, Y.H., P.M., R.D. and F.T.; Formal analysis, Y.H., P.M., R.D. and F.T.; Investigation, Y.H., P.M. and F.T.; Validation, P.M., R.D. and F.T.; Writing—Original Draft, Y.H., P.M., R.D. and F.T.; Writing—Review & Editing, R.D. and F.T. All authors have read and agreed to the published version of the manuscript.

Funding: This research received no external funding.

Conflicts of Interest: The authors declare no conflict of interest.

References

1. Lord, H.W.; Shulman, Y. A generalized dynamical theory of thermoelasticity. *J. Mech. Phys. Solids* **1967**, *15*, 299–309. [[CrossRef](#)]
2. Hetnarski, R.B.; Ignaczak, J. Generalized thermoelasticity. *J. Therm. Stresses* **1999**, *22*, 451–476.
3. Chouduri, S.K.R. On a thermoelastic three-phase-lag model. *J. Therm. Stresses* **2007**, *30*, 231–238. [[CrossRef](#)]
4. Bahtui, A.; Eslami, M.R. Generalized coupled thermoelasticity of functionally graded cylindrical shells. *Int. J. Numer. Methods Eng.* **2007**, *69*, 676–697. [[CrossRef](#)]
5. Bagri, A.; Eslami, M.R. Generalized coupled thermoelasticity of functionally graded annular disk considering the Lord–Shulman theory. *Compos. Struct.* **2008**, *83*, 168–179. [[CrossRef](#)]
6. Zhou, F.-X.; Li, S.; Lai, Y.-M. Three-dimensional analysis for transient coupled thermoelastic response of a functionally graded rectangular plate. *J. Sound Vib.* **2011**, *330*, 3990–4001. [[CrossRef](#)]
7. Shariyat, M. Nonlinear transient stress and wave propagation analyses of the FGM thick cylinders, employing a unified generalized thermoelasticity theory. *Int. J. Mech. Sci.* **2012**, *65*, 24–37. [[CrossRef](#)]
8. Abbas, I.A.; Zenkour, A.M. LS model on electro–magneto–thermoelastic response of an infinite functionally graded cylinder. *Compos. Struct.* **2013**, *96*, 89–96. [[CrossRef](#)]
9. Xia, R.; Tian, X.; Shen, Y. Dynamic response of two-dimensional generalized thermoelastic coupling problem subjected to a moving heat source. *Acta Mech. Solida Sin.* **2014**, *27*, 300–305. [[CrossRef](#)]
10. Zenkour, A.M. Three-dimensional thermal shock plate problem within the framework of different thermoelasticity theories. *Compos. Struct.* **2015**, *132*, 1029–1042. [[CrossRef](#)]
11. Heydarpour, Y.; Aghdam, M.M. Transient analysis of rotating functionally graded truncated conical shells based on the Lord–Shulman model. *Thin Walled Struct.* **2016**, *104*, 168–184. [[CrossRef](#)]
12. Kiani, Y.; Eslami, M.R. Nonlinear generalized thermoelasticity of an isotropic layer based on Lord–Shulman theory. *Eur. J. Mech. Solids* **2017**, *61*, 245–253. [[CrossRef](#)]
13. Entezari, A.; Filippi, M.; Carrera, E.; Kouchakzadeh, M.A. 3D dynamic coupled thermoelastic solution for constant thickness disks using refined 1D finite element models. *Appl. Math. Model.* **2018**, *60*, 273–285. [[CrossRef](#)]
14. Wang, Y.Z.; Zan, C.; Liu, D.; Zhou, J.Z. Generalized solution of the thermoelastic problem for the axisymmetric structure with temperature-dependent properties. *Eur. J. Mech. Solids* **2019**, *76*, 346–354. [[CrossRef](#)]
15. Ootao, Y.; Tanigawa, Y. Two-dimensional thermoelastic analysis of a functionally graded cylindrical panel due to nonuniform heat supply. *Mech. Res. Commun.* **2005**, *32*, 429–443. [[CrossRef](#)]
16. Shao, Z.S.; Wang, T.J. Three-dimensional solutions for the stress fields in functionally graded cylindrical panel with finite length and subjected to thermal/mechanical loads. *Int. J. Solids Struct.* **2006**, *43*, 3856–3874. [[CrossRef](#)]
17. Ootao, Y.; Tanigawa, Y. Transient thermoelastic problem of a functionally graded cylindrical panel due to nonuniform heat supply. *J. Therm. Stresses* **2007**, *30*, 441–457. [[CrossRef](#)]
18. Shao, Z.; Wang, T.; Ang, K.K. Transient thermomechanical stresses of functionally graded cylindrical panels. *AIAA J.* **2007**, *45*, 2487–2496. [[CrossRef](#)]
19. Wang, X.; Sudak, L.J. Three-dimensional analysis of multi-layered functionally graded anisotropic cylindrical panel under thermomechanical loading. *Mech. Mater.* **2008**, *40*, 235–254. [[CrossRef](#)]
20. Malekzadeh, P.; Ghaedsharaf, M. Three-dimensional thermoelastic analysis of finite length laminated cylindrical panels with functionally graded layers. *Meccanica* **2014**, *49*, 887–906. [[CrossRef](#)]
21. Ranjan Kar, V.; Kumar Panda, S. Thermoelastic analysis of functionally graded doubly curved shell panels using nonlinear finite element method. *Compos. Struct.* **2015**, *129*, 201–212.
22. Khakpour Komarsofla, M.; Jedari Salami, S.; Shakeri, M. Thermo elastic- up to yielding behavior of three dimensional functionally graded cylindrical panel based on a full layer-wise theory. *Compos. Struct.* **2019**, *208*, 261–275. [[CrossRef](#)]
23. Kumar Hirwani, C.; Kumar Panda, S. Nonlinear finite element solutions of thermoelastic deflection and stress responses of internally damaged curved panel structure. *Appl. Math. Model.* **2019**, *65*, 303–317. [[CrossRef](#)]
24. Wu, C.-P.; Huang, S.-E. Three-dimensional solutions of functionally graded piezo-thermo-elastic shells and plates using a modified pagano method. *Comput. Mater. Contin.* **2009**, *12*, 251–281.

25. Wu, C.-P.; Chiu, K.-H.; Jiang, R.-Y. A meshless collocation method for the coupled analysis of functionally graded piezo-thermo-elastic shells and plates under thermal loads. *Int. J. Eng. Sci.* **2012**, *56*, 29–48. [[CrossRef](#)]
26. Sheng, G.G.; Wang, X. Response and control of functionally graded laminated piezoelectric shells under thermal shock and moving loadings. *Compos. Struct.* **2010**, *93*, 132–141. [[CrossRef](#)]
27. Alibeigloo, A. Thermoelastic solution for static deformations of functionally graded cylindrical shell bonded to thin piezoelectric layers. *Compos. Struct.* **2011**, *93*, 961–972. [[CrossRef](#)]
28. Akbari Alashti, R.; Khorsand, M. Three-dimensional dynamo-thermo-elastic analysis of a functionally graded cylindrical shell with piezoelectric layers by DQ-FD coupled. *Int. J. Press. Vessel. Pip.* **2012**, *96–97*, 49–67. [[CrossRef](#)]
29. Akbari Alashti, R.; Khorsand, M. Three-dimensional nonlinear thermo-elastic analysis of functionally graded cylindrical shells with piezoelectric layers by differential quadrature method. *Acta Mech.* **2012**, *223*, 2565–2590. [[CrossRef](#)]
30. Alibeigloo, A. Thermoelastic analysis of functionally graded carbon nanotube reinforced composite cylindrical panel embedded in piezoelectric sensor and actuator layers. *Compos. Part B Eng.* **2016**, *98*, 225–243. [[CrossRef](#)]
31. Alibeigloo, A.; Pasha Zanoosi, A.A. Thermo-electro-elasticity solution of functionally graded carbon nanotube reinforced composite cylindrical shell embedded in piezoelectric layers. *Compos. Struct.* **2017**, *173*, 268–280. [[CrossRef](#)]
32. Entezari, A.; Filippi, M.; Carrera, E.; Kouchakzadeh, M.A. 3D-wave propagation in generalized thermoelastic functionally graded disks. *Compos. Struct.* **2018**, *206*, 941–951. [[CrossRef](#)]
33. Zhang, X.-Y.; Xie, Y.-J.; Li, X.-F. Transient thermoelastic response in a cracked strip of functionally graded materials via generalized fractional heat conduction. *Appl. Math. Model.* **2019**, *70*, 328–349. [[CrossRef](#)]
34. Sator, L.; Sladek, V.; Sladek, J. Coupling effects in transient analysis of FGM plates bending in non-classical thermoelasticity. *Compos. Part B Eng.* **2019**, *165*, 233–246. [[CrossRef](#)]
35. Poursaghar, A.; Chen, Z. Hyperbolic heat conduction and thermoelastic solution of functionally graded CNT reinforced cylindrical panel subjected to heat pulse. *Int. J. Solids Struct.* **2019**, *163*, 117–129. [[CrossRef](#)]
36. Heydarpour, Y.; Malekzadeh, P. Thermoelastic analysis of multilayered FG spherical shells based on Lord-Shulman theory. *Iran. J. Sci. Technol. Trans. Mech. Eng.* **2019**, *43*, 845–867. [[CrossRef](#)]
37. Heydarpour, Y.; Malekzadeh, P.; Gholipour, F. Thermoelastic analysis of FG-GPLRC spherical shells under thermo-mechanical loadings based on Lord-Shulman theory. *Compos. Part B Eng.* **2019**, *164*, 400–424. [[CrossRef](#)]
38. Golbahar Haghighi, M.; Malekzadeh, P.; Rahideh, H.; Vaghefi, M. Inverse transient heat conduction problems of a multilayered functionally graded cylinder. *Numer. Heat Transfer Part A Appl.* **2012**, *61*, 717–733. [[CrossRef](#)]
39. Arefi, M.; Mohammadi, M.; Tabatabaeian, A.; Dimitri, R.; Tornabene, F. Two-dimensional thermo-elastic analysis of FG-CNTRC cylindrical pressure vessels. *Steel Compos. Struct.* **2018**, *27*, 525–536.
40. Karami, B.; Shahsavari, D.; Janghorban, M.; Dimitri, R.; Tornabene, F. Wave propagation of porous nanoshells. *Nanomaterials* **2018**, *9*, 22. [[CrossRef](#)]
41. Mohammadi, M.; Arefi, M.; Dimitri, R.; Tornabene, F. Higher-order thermo-elastic analysis of FG-CNTRC cylindrical vessels surrounded by a pasternak foundation. *Nanomaterials* **2019**, *9*, 79. [[CrossRef](#)] [[PubMed](#)]
42. Nejati, M.; Ghasemi-Ghalebahman, A.; Soltanimaleki, A.; Dimitri, R.; Tornabene, F. Thermal vibration analysis of SMA hybrid composite double curved sandwich panels. *Compos. Struct.* **2019**, *224*, 111035. [[CrossRef](#)]
43. Malekzadeh, P. A two-dimensional layerwise-differential quadrature static analysis of thick laminated composite circular arches. *Appl. Math. Model.* **2009**, *33*, 1850–1861. [[CrossRef](#)]
44. Malekzadeh, P.; Golbahar Haghighi, M.R.; Heydarpour, Y. Heat transfer analysis of functionally graded hollow cylinders subjected to an axisymmetric moving boundary heat flux. *Numer. Heat Transfer Part A Appl.* **2012**, *61*, 614–632. [[CrossRef](#)]
45. Heydarpour, Y.; Aghdam, M.M. A hybrid Bézier based multi-step method and differential quadrature for 3D transient response of variable stiffness composite plates. *Compos. Struct.* **2016**, *154*, 344–359. [[CrossRef](#)]
46. Dimitri, R.; Fantuzzi, N.; Tornabene, F.; Zavarise, G. Innovative numerical methods based on SFEM and IGA for computing stress concentrations in isotropic plates with discontinuities. *Int. J. Mech. Sci.* **2016**, *118*, 166–187. [[CrossRef](#)]
47. Kamarian, S.; Salim, M.; Dimitri, R.; Tornabene, F. Free vibration analysis of conical shells reinforced with agglomerated Carbon Nanotubes. *Int. J. Mech. Sci.* **2016**, *108–109*, 157–165. [[CrossRef](#)]

48. Tornabene, F.; Dimitri, R.; Viola, E. Transient dynamic response of generally-shaped arches based on a GDQ-time-stepping method. *Int. J. Mech. Sci.* **2016**, *114*, 277–314. [[CrossRef](#)]
49. Nejati, M.; Asanjarani, A.; Dimitri, R.; Tornabene, F. Static and free vibration analysis of functionally graded conical shells reinforced by carbon nanotubes. *Int. J. Mech. Sci.* **2017**, *130*, 383–398. [[CrossRef](#)]
50. Heydarpour, Y.; Aghdam, M.M. A coupled integral–differential quadrature and B-spline-based multi-step technique for transient analysis of VSCL plates. *Acta Mech.* **2017**, *228*, 2965–2986. [[CrossRef](#)]
51. Malekzadeh, P.; Setoodeh, A.R.; Shojaee, M. Vibration of FG-GPLs eccentric annular plates embedded in piezoelectric layers using a transformed differential quadrature method. *Comput. Meth. Appl. Mech. Eng.* **2018**, *340*, 451–479. [[CrossRef](#)]
52. Heydarpour, Y.; Aghdam, M.M. Response of VSCL plates under moving load using a mixed integral-differential quadrature and novel NURBS based multi-step method. *Compos. Part B Eng.* **2018**, *140*, 260–280. [[CrossRef](#)]
53. Santos, H.; Mota Soares, C.M.; Mota Soares, C.A.; Reddy, J.N. A semi-analytical finite element model for the analysis of cylindrical shells made of functionally graded materials under thermal shock. *Compos. Struct.* **2008**, *86*, 10–21. [[CrossRef](#)]



© 2020 by the authors. Licensee MDPI, Basel, Switzerland. This article is an open access article distributed under the terms and conditions of the Creative Commons Attribution (CC BY) license (<http://creativecommons.org/licenses/by/4.0/>).